J. Plasma Physics (2000), *vol.* 64, *part* 1, *pp.* 57–74. Printed in the United Kingdom

© 2000 Cambridge University Press

Spatial absorption of a magnetosonic wave in a dusty magnetized plasma

M. C. de JULI and R. S. SCHNEIDER

Instituto de Física, Universidade Federal do Rio Grande do Sul, Caixa Postal 15051, 91501-970 Porto Alegre, RS, Brasil (juli@if.ufrgs.br)

(Received 20 July 1999 and in revised form 28 January 2000)

Abstract. The dielectric tensor for a multicomponent magnetized dusty plasma, including the effect of capture of plasma electrons and ions by the dust particles, is rewritten in order to provide expressions more suitable for applications. We use this tensor to study the spatial absorption of a magnetosonic wave, including effects up to second order in the Larmor radius. We analyse the absorption of the wave due to the presence of dust particles with variable charge and the modification of this absorption due to finite-Larmor-radius effects.

1. Introduction

In a previous paper (de Juli and Schneider 1998, hereinafter referred to as paper I), we developed a kinetic theory of a dusty magnetized plasma with variable charge on the dust particles. The dielectric tensor was written as the sum of two terms. One term has components $\tilde{\epsilon}^h_{ij}$, and is formally identical with the dielectric tensor of a homogeneous magnetized plasma, with the resonant denominator modified by the addition of a purely imaginary term containing a frequency $\nu^0_{\beta d}$ that characterizes the collisions between plasma particles and dust particles. The other term, with components ϵ^N_{ij}, is entirely dependent on the model used to describe the charging process of the dust particles.

In this paper, we rewrite the components of this dielectric tensor in a new form, using a convenient expansion of the Bessel functions, in order to deal more easily with the different powers of the Larmor radius, which are essential for the analysis of the effects of charge variation of the dust particles that are included in ϵ^N_{ij}.

We use this tensor to study the propagation of a magnetosonic wave in a dusty magnetized plasma with the variation of the charge of the dust taken into account, and to analyse how the spatial propagation of this wave is influenced by the presence of the dust in the plasma and by the change in the dust charge. We show that spatial absorption occurs owing to the charge variation of the dust particles. This absorption is not significantly changed by contributions connected with finite-Larmor-radius effects included in ϵ^N_{ij}.

2. The dielectric tensor

In paper I, we obtained the components of the dielectric tensor for a homogeneous dusty magnetized plasma. We consider again a homogeneous plasma composed of particles of charge q_β and mass m_β, where the subscript

https://doi.org/10.1017/S0022377800008448 Published online by Cambridge University Press

$\beta = e$, i identifies electrons and ions respectively, in a homogeneous magnetic field $\mathbf{B_0} = B_0\,\mathrm{e}_z$. In this magnetized plasma, we consider embedded spherical dust grains with radius a and variable charge q; the charge variation originates from collisions between the dust particles and particles of species β. The assumption of spherical dust grains is valid in the limit $a \ll \lambda_D \ll \lambda_{\mathrm{mfp}}$, where λ_D is the plasma Debye length and λ_{mfp} is the mean free path of electrons and ions.

We are considering Larmor-radius effects arising from the motion of electrons and ions and neglecting this kind of effect for the dust particles, since they are assumed to be immobile because of their large mass. This assumption implies that the regime in which our work is valid is such that $\omega \gg \Omega_d$, where Ω_d is the cyclotron frequency of the dust particles.

At the same time, we neglect the influence of the external magnetic field in the charging process of the dust particles, using a cross-section for this process derived from the OML theory (Tsytovich 1997). This is based on a numerical calculation by Chang and Spariosu (1993), which shows that the characteristics of the dust-particles charging process are not significantly influenced by the presence of an external magnetic field if the dust-particle radius $a < \rho_G$, where ρ_G is the mean gyroradius of the electrons, given by $\rho_G = (\frac{1}{2}\pi)^{1/2} r_{Le}$, with r_{Le} the electron Larmor radius. For the parameter values used in this work, the relation $a < \rho_G$ is always satisfied.

The components of the dielectric tensor are written as $\epsilon_{ij} = \tilde{\epsilon}^h_{ij} + \epsilon^N_{ij}$. The first term is given by

$$\tilde{\epsilon}^h_{ij} = \delta_{ij} + \hat{\epsilon}^h_{ij} - \delta_{iz}\,\delta_{jz} \sum_\beta \frac{X_\beta}{n_{\beta 0}} \int d^3u\, \frac{u_\parallel}{u_\perp} L(F_{\beta 0}) + \delta_{jz} \sum_\beta \frac{X_\beta}{n_{\beta 0}} \sum_{n=-\infty}^{\infty} \int d^3\,u \left[i \frac{\nu^0_{\beta d}(u)}{\omega} \frac{L(F_{\beta 0})}{D_{n\beta}} \left(\frac{u_\parallel}{u_\perp} \right)^{\delta_{iz}} \right] R^{n\beta}_{ij}, \tag{2.1}$$

with

$$\hat{\epsilon}^h_{ij} = \sum_\beta \frac{X_\beta}{n_{\beta 0}} \sum_{n=-\infty}^{\infty} \int d^3u\, u_\perp \frac{\mathscr{L}(F_{\beta 0})}{D_{n\beta}} \left(\frac{u_\parallel}{u_\perp} \right)^{\delta_{iz}+\delta_{jz}} R^{n\beta}_{ij}. \tag{2.2}$$

In these expressions, $\mathbf{u} = \mathbf{p}/m_\beta c$, $X_\beta = \omega^2_{p\beta}/\omega^2, \omega^2_{p\beta} = 4\pi n_{\beta 0} q^2_\beta / m_\beta$ is the square of the plasma frequency of particles of species β, $n_{\beta 0}$ and $F_{\beta 0}$ are the equilibrium density and the equilibrium distribution function respectively of particles of species β,

$$\mathscr{L}(F_{\beta 0}) = \frac{1}{\gamma_\beta} \left[(\gamma_\beta - N_\parallel u_\parallel) \frac{\partial F_{\beta 0}}{\partial u_\perp} + N_\parallel u_\perp \frac{\partial F_{\beta 0}}{\partial u_\parallel} \right], \tag{2.3}$$

with $N_\parallel = k_\parallel c/\omega$, γ_β being the relativistic factor, and

$$L(F_{\beta 0}) = \frac{1}{\gamma_\beta} \left(u_\parallel \frac{\partial F_{\beta 0}}{\partial u_\perp} - u_\perp \frac{\partial F_{\beta 0}}{\partial u_\parallel} \right). \tag{2.4}$$

Also,

$$D_{n\beta} = \gamma_\beta \left(1 + i \frac{\nu^0_{\beta d}}{\omega} \right) - N_\parallel u_\parallel - n Y_\beta, \tag{2.5}$$

where

$$\nu^0_{\beta d} = \pi a^2 n_{d0}\, c \frac{u^2 + \tilde{C}_\beta}{u} H(u^2 + \tilde{C}_\beta), \qquad \tilde{C}_\beta \equiv \frac{2 Z_d\, e q_\beta}{a m_\beta c^2},$$

$-Z_d\, e$ being the equilibrium charge of the dust particle and H the Heaviside function, and $Y_\beta = \Omega_\beta/\omega$ where $\Omega_\beta = q_\beta B_0/m_\beta c$ is the cyclotron frequency of

https://doi.org/10.1017/S0022377800008448 Published online by Cambridge University Press

particles of species β. The $R_{ij}^{n\beta}$ are combinations of Bessel functions with argument $b_\beta = N_\perp u_\perp / Y_\beta$, where $N_\perp = k_\perp c/\omega$, and their derivatives. Full expressions for the $R_{ij}^{n\beta}$ are given in Appendix A.

The second term of the tensor is given by

$$\epsilon_{ij}^N = -\frac{4\pi i}{\omega}\frac{c^2}{\omega^2}\frac{1}{1+i\left(\frac{\nu_d^0}{\omega}+\frac{\nu_1}{\omega}\right)}\hat{U}_i\hat{S}_j, \tag{2.6}$$

where

$$\hat{U}_i = \sum_\beta q_\beta \sum_{n=-\infty}^{\infty}\int d^3u\, u_\perp \frac{u\sigma'(u)F_{\beta 0}}{g_\beta - nY_\beta}\left(\frac{u_\parallel}{u_\perp}\right)^{\delta_{iz}} R_{iz}^{n\beta} \tag{2.7}$$

and

$$\begin{aligned}\hat{S}_j = &\sum_\beta \frac{q_\beta^2}{m_\beta c}\sum_{n=-\infty}^{\infty}\int d^3u \frac{[i\nu_{\beta d}^0(u)/\omega]\,\mathscr{L}(F_{\beta 0})}{g_\beta - nY_\beta}\left(\frac{u_\parallel}{u_\perp}\right)^{\delta_{jz}} R_{zj}^{n\beta}\\ &-\delta_{jz}\sum_\beta \frac{q_\beta^2}{m_\beta c}\int d^3u\left[i\frac{\nu_{\beta d}^0(u)}{\omega}\frac{L(F_{\beta 0})}{u_\perp}\right]\\ &+\delta_{jz}\sum_\beta \frac{q_\beta^2}{m_\beta c}\sum_{n=-\infty}^{\infty}\int d^3u \frac{[i\nu_{\beta d}^0(u)/\omega]^2}{g_\beta - nY_\beta}\frac{L(F_{\beta 0})}{u_\perp}R_{zj}^{n\beta}.\end{aligned} \tag{2.8}$$

In these expressions,

$$\nu_d^0 = -c\sum_\beta q_\beta \int d^3u\, \sigma'_\beta u F_{\beta 0}, \tag{2.9}$$

where $\sigma'_\beta(u) \equiv (\partial\sigma_\beta/\partial q)|_{q=-z_d e}$, and the charging cross-section is given (Spitzer 1978) by

$$\sigma_\beta(q,u) = \pi a^2\left(1-\frac{q}{Z_d e}\frac{\tilde{C}_\beta}{u^2}\right)H\left(1-\frac{q}{Z_d e}\frac{\tilde{C}_\beta}{u^2}\right). \tag{2.10}$$

Also,

$$\nu_1 = ic\sum_\beta q_\beta \sum_{n=-\infty}^{\infty}\int d^3u \frac{\nu_{\beta d}^0}{\omega}\gamma_\beta u\sigma'_\beta F_{\beta 0}\frac{J_n^2(b_\beta)}{g_\beta - nY_\beta}, \tag{2.11}$$

where

$$g_\beta \equiv \gamma_\beta\left(1+i\frac{\nu_{\beta d}^0}{\omega}\right) - N_\parallel u_\parallel.$$

This form of the dielectric tensor is very general, under the assumptions that we have made, and was used in paper I to study the propagation of a magnetosonic wave perpendicularly to the external magnetic field. In doing this, in order to evaluate the integrals in the u variable, we make an expansion of the denominator that occurs in them, and which is very common in the literature (Vladimirov 1994; Prasad 1998). This kind of expansion is good if the involved frequencies are sufficiently high that $\omega \sim \omega_{pe} \gg \max(kv_{Te}, \nu_d^0, \nu_{\beta d}^0)$ (Vladimirov 1994), and has as consequence that only a few terms need be retained. If the frequency is lowered, we must retain more and more terms in the expansion, which turns out to be algebraically very expensive. A better approach is to rewrite the general dielectric tensor in a form that is more convenient for regimes with lower frequencies and that at the same time takes care of powers of the Larmor radius in an easy way.

https://doi.org/10.1017/S0022377800008448 Published online by Cambridge University Press

In order to rewrite this tensor in a more suitable form for application, in all these expressions the summation over n from minus to plus infinity is transformed into a summation running from zero to infinity, and the combinations of Bessel functions and their derivatives are expanded in the following way (Abramowitz and Stegun 1970):

$$J_n^2(b_\beta) = \sum_{m=0}^{\infty} a(n,m)\,(b_\beta^2)^{n+m}, \tag{2.12}$$

$$J_n(b_\beta)\,J_n'(b_\beta) = \sum_{m=0}^{\infty} (n+m)\,a(n,m)\,b_\beta (b_\beta^2)^{n+m-1}, \tag{2.13}$$

$$J_n'^2(b_\beta) = \sum_{m=0}^{\infty} d(n,m)\,(b_\beta^2)^{n+m-1}, \tag{2.14}$$

where

$$a(n,m) = \frac{(-1)^m[2(n+m)]!\,(\frac{1}{2})^{2(n+m)}}{[(n+m)!]^2(2n+m)!\,m!}, \tag{2.15}$$

and $d(n,m) = a(1,m-2)$ for $n = 0$, and

$$d(n,m) = \frac{1}{4}\left[a(n-1,m)+a(n+1,m-2)-2\frac{n+m-1}{n+m}a(n,m-1)\right] \tag{2.16}$$

for $n > 0$, with the convention $1/(-m)! = 0$.

Then all the components of the dielectric tensor for the wavevector $\mathbf{k}$ in the (x,z) plane can be written in terms of integrals of the form

$$\tilde{I}_\beta(n,m,h,s;G) \equiv \frac{1}{n_{\beta 0}}\int d^3u\,\frac{u_\parallel^h\,u_\perp^{2(n+m-1)}u_\perp\,G}{g_\beta + sn Y_\beta}. \tag{2.17}$$

Using (2.12)–(2.14), the components $\tilde{\epsilon}_{ij}^h$ and ϵ_{ij}^N of the dielectric tensor can be written as series in powers of $N_\perp/Y_\beta$, where in each term we have an integral of the type (2.17). The full expressions for $\tilde{\epsilon}_{ij}^h$ and ϵ_{ij}^N are given in Appendix B.

3. The magnetosonic wave

The dispersion relation for the magnetosonic wave, which propages perpendicularly to the external magnetic field ($N_\parallel = 0$), can be written formally as

$$\Lambda \equiv N^2 - \frac{\epsilon_{xx}\,\epsilon_{yy} - \epsilon_{xy}\,\epsilon_{yx}}{\epsilon_{xx}} = 0. \tag{3.1}$$

We shall use for the equilibrium distribution functions of electrons and ions, Maxwellian distribution functions

$$F_{\beta 0} = \frac{\mu_\beta^{3/2} n_{\beta 0}}{(2\pi)^{3/2}} e^{-\mu_\beta u^2/2},$$

https://doi.org/10.1017/S0022377800008448 Published online by Cambridge University Press

where $\mu_\beta = m_\beta c^2/T_\beta$, T_β being the temperature of particles of species β, with $T_e = T_i = T$. The following approximations are made in the calculation of the components of interest of the dielectric tensor presented in Sect. 2: relativistic effects are neglected, which means that $\gamma_\beta \approx 1$; in each component of the dielectric tensor, we retain only contributions up to order N^2, which implies retaining only the lowest-order contributions in the finite Larmor radius. We obtain all the necessary components of the dielectric tensor in terms of the integrals

$$i_n \equiv \int_0^{\sqrt{-\tilde{C}_e}} du\, u^n e^{-\mu_e u^2/2}, \tag{3.2}$$

$$I(p,n) \equiv \int_0^\infty du\, \frac{u^n e^{-\mu_i u^2/2}}{(1+pY_i)^2 u^2 + A^2(u^2+\tilde{C}_i)^2}, \tag{3.3}$$

$$E(p,n) \equiv \int_{\sqrt{-\tilde{C}_e}}^\infty du\, \frac{u^n e^{-\mu_e u^2/2}}{(1+pY_e)^2 u^2 + A^2(u^2+\tilde{C}_e)^2}, \tag{3.4}$$

where $A \equiv \pi a^2 n_{d0} c/\omega$. The dielectric tensor components of interest for the dispersion relation under consideration, written as $\epsilon_{ij} = \tilde{\epsilon}^h_{ij} + \epsilon^N_{ij}$, will be rewritten in such a way as to make clear the dependence on N^2. The terms $\tilde{\epsilon}^h_{ij}$ are given by

$$\tilde{\epsilon}^h_{xx} = (1 + \chi^{0R}_{xx} + N^2\chi^{1R}_{xx}) + i(\chi^{0I}_{xx} + N^2\chi^{1I}_{xx}), \tag{3.5}$$

$$\tilde{\epsilon}^h_{yy} = \tilde{\epsilon}^h_{xx} + N^2(\chi^{1R}_{yy} + i\chi^{1I}_{yy}), \tag{3.6}$$

$$\tilde{\epsilon}^h_{xy} = (\chi^{0R}_{xy} + N^2\chi^{1R}_{xy}) + i(\chi^{0I}_{xy} + N^2\chi^{1I}_{xy}), \tag{3.7}$$

and $\tilde{\epsilon}^h_{yx} = \tilde{\epsilon}^{h*}_{xy}$, where the expressions for the χ^{0R}_{ij} and χ^{0I}_{ij} are given in Appendix C.

The components ϵ^N_{ij} can be written as

$$\epsilon^N_{xx} = N^2 C(\chi^{NR}_{xx} + i\chi^{NI}_{xx}), \tag{3.8}$$

$$\epsilon^N_{yy} = -N^2 C(\chi^{NR}_{yy} + i\chi^{NI}_{yy}), \tag{3.9}$$

$$\epsilon^N_{xy} = -N^2 C(\chi^{NR}_{xy} + i\chi^{NI}_{xy}), \tag{3.10}$$

$$\epsilon^N_{yx} = -N^2 C(\chi^{NR}_{yx} + i\chi^{NI}_{yx}). \tag{3.11}$$

In these expressions,

$$C \equiv \frac{1}{36\omega^4} \frac{n_{d0}\, a^3}{d_r^2 + d_i^2} \tag{3.12}$$

and

$$\chi^{NR}_{ij} = \hat{A} F^R_{ij} - \hat{B} F^I_{ij} \tag{3.13}$$

$$\chi^{NI}_{ij} = \hat{B} F^R_{ij} + \hat{A} F^I_{ij}, \tag{3.14}$$

where

$$\hat{A} \equiv d_i + (d_r - d_i)\,\delta_{ij}, \tag{3.15}$$

$$\hat{B} \equiv d_r - (d_r + d_i)\,\delta_{ij}, \tag{3.16}$$

https://doi.org/10.1017/S0022377800008448 Published online by Cambridge University Press

δ_{ij} is the Kronecker delta, and

$$d_r = 1 - \frac{\nu_1^I}{\omega}, \qquad d_i = \frac{\nu_d^0}{\omega} + \frac{\nu_1^R}{\omega},$$

with

$$\nu_d^0 = \frac{a}{c(2\pi)^{1/2}} (\omega_{pi}^2 \mu_i^{1/2} + \omega_{pe}^2 \mu_e^{1/2} e^{-Z_d e^2/Ta}), \tag{3.17}$$

$$\nu_1^R = -\frac{A}{\omega} \left(\frac{\pi}{2}\right)^{1/2} n_{d0}\, a^3 \{\omega_{pi}^2 \mu_i^{3/2} [I(0,5) + 2\tilde{C}_i I(0,3) + \tilde{C}_i^2 I(0,1)] + \omega_{pe}^2 \mu_e^{3/2} [E(0,5) + 2\tilde{C}_e E(0,3) + \tilde{C}_e^2 E(0,1)]\}, \tag{3.18}$$

$$\nu_1^I = -\frac{1}{\omega} \left(\frac{\pi}{2}\right)^{1/2} n_{d0}\, a^3 \{\omega_{pi}^2 \mu_i^{3/2} [I(0,4) + \tilde{C}_i I(0,2)] + \omega_{pe}^2 \mu_e^{3/2} [E(0,4) + \tilde{C}_e E(0,2)]\}. \tag{3.19}$$

The full expressions for the F_{ij}^R and F_{ij}^I are given in Appendix D.

4. Numerical results

In this section, we present a numerical analysis of the effects of the dust particles with variable charge on the propagation properties of the magnetosonic wave. The two main effects to be investigated are those due to the modelling of the charge variation of the dust particles and those due to finite-Larmor-radius effects of electrons and ions. The plasma parameters will be chosen in the range of typical values for laboratory and astrophysical plasmas.

We recall that in paper I, we also analysed the propagation properties of the magnetosonic wave, but restricted to the cold-plasma limit, and using a real wavevector **k** and a complex frequency ω. In the application developed in paper I, very early on we made the assumption that $\omega \ll \Omega_i$, and also made several expansions of denominators of integrands that occur in the components of the dielectric tensor and are currently used in the literature (Prasad 1998). In the present paper, these expansions are not made, and we are interested also in making a comparison between the two ways of calculating the dielectric tensor. The expressions obtained in the present paper for the dispersion relation of the magnetosonic wave are valid for $\omega \gg \Omega_d$, because the motion of the dust particles is not considered in the model here proposed.

We note that in Figs 1–6, the frequencies are in the range $\Omega_d \ll \omega < \Omega_i$, because we are mainly interested in the magnetosonic wave without the effects of finite ion-cyclotron frequency being taken into account; in Figs 7 and 8 we use the range $\Omega_d \ll \omega \leqslant 2\Omega_i$, because we are interested in the behaviour of the refractive index for frequencies near the ion-cyclotron frequency.

Initially, we show the results obtained using the cold-plasma approximation and the technique of expansion of the denominators used in paper I, assuming real ω and complex k.

In Figs 1 and 2, we show the real part of the refractive index, $N_r = ck_r/\omega$, and the complex part, $N_i = ck_i/\omega$, respectively, as functions of the wave frequency

https://doi.org/10.1017/S0022377800008448 Published online by Cambridge University Press

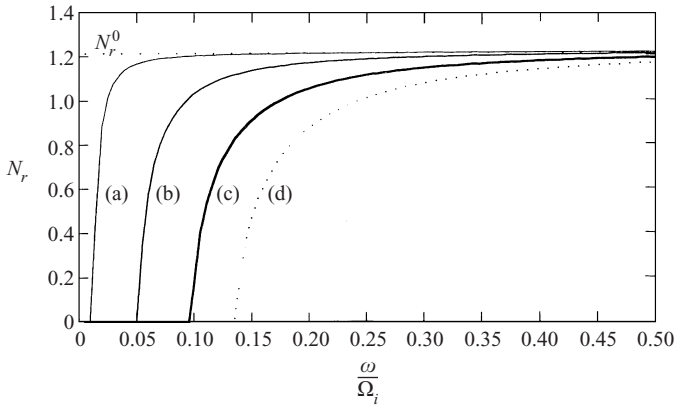


Figure 1. N_r as a function of ω/Ω_i, calculated as in paper I, for several values of $T = T_e = T_i$. Curves (a), (b), (c) and (d) correspond to $T = 0.25$, 1, 2 and 3 eV respectively. The fixed parameters are $n_{i0} = 10^8$ cm^{-3}, $a = 10^{-4}$ cm, $n_{d0} = 10^4$ cm^{-3} and $B_0 = 0.2$ T. The curve N_r^0 correspond to the refractive index in the absence of dust particles.

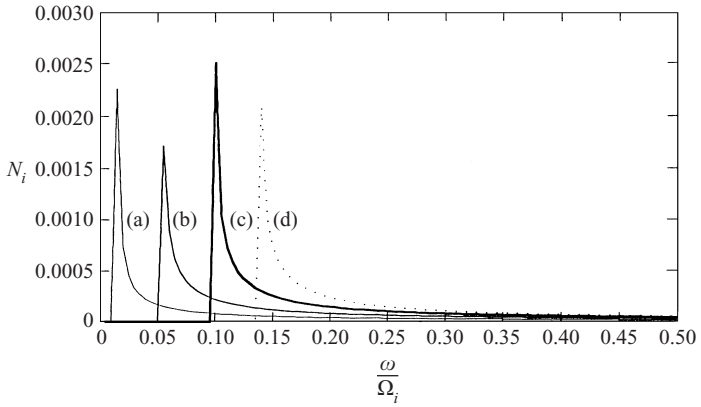


Figure 2. N_i as a function of ω/Ω_i, calculated as in paper I, for several values of $T = T_e = T_i$. Curves (a), (b), (c) and (d) correspond to $T = 0.25$, 1, 2 and 3 eV respectively, and the other parameters are the same as in Fig. 1.

normalized to the ion-cyclotron frequency ω/Ω_i, for several values of the temperature $T = T_e = T_i$. Curves (a), (b), (c) and (d) correspond to $T = 0.25$, 1, 2 and 3 eV respectively. The fixed parameters are $n_{i0} = 10^8$ cm^{-3}, $a = 10^{-4}$ cm, $n_{d0} = 10^4$ cm^{-3} and $B_0 = 0.2$ T. These figures are obtained from the following expressions derived from paper I:

$$N_r^2 = \mathscr{A}[1 - F(\omega)], \tag{4.1}$$

$$2N_r N_i = \frac{\mathscr{B}}{\omega}[1 + F(\omega)], \tag{4.2}$$

where

$$F(\omega) = \frac{\mathscr{C}^2}{\mathscr{A}^2\omega^2 + \mathscr{B}^2}, \tag{4.3}$$

https://doi.org/10.1017/S0022377800008448 Published online by Cambridge University Press

and

$$\mathscr{A} \equiv 1+\sum_{\beta}\frac{\omega_{p\beta}^2}{\Omega_{\beta}^2}\approx 1+\frac{c^2}{V_{Ai}^2}, \tag{4.4}$$

$$\mathscr{B} \equiv \frac{4a^2 n_{d0}}{3}\sqrt{2\pi}\sum_{\beta}\frac{\omega_{p\beta}^2}{\Omega_{\beta}^2}u_{T\beta}\left(2+\frac{Z_d e^2}{Ta}\right)\left[\delta_{\beta i}+\exp\left(-\frac{Z_d e^2}{Ta}\right)\delta_{\beta e}\right], \tag{4.5}$$

$$\mathscr{C} \equiv \sum_{\beta}\frac{\omega_{p\beta}^2}{\Omega_{\beta}}=\frac{4\pi}{B_0}Z_d e n_{d0}. \tag{4.6}$$

The cutoff of the real part of the refractive index, which appears in Fig. 1, occurs when $F(\omega)=1$, which gives for the cutoff frequency ω_c the value

$$\left(\frac{\omega_c}{\Omega_i}\right)^2=\frac{\mathscr{C}^2-\mathscr{B}^2}{\mathscr{A}^2\Omega_i^2}. \tag{4.7}$$

Because in this expression only $\mathscr{B}$ depends on the temperature and this dependence is approximately proportional to $1/T$, when T increases, $\mathscr{B}$ diminishes and ω_c increases, in agreement with Fig. 1.

When the dust particles are absent ($n_{d0}=0$) or when their charges are fixed ($\mathscr{B}=0$), we have

$$N_r^0=\mathscr{A}^{1/2}\approx\left(1+\frac{4\pi c^2 n_{i0}m_i}{B_0}\right)^{1/2}, \tag{4.8}$$

where N_r^0 indicates the real part of the refractive index in the absence of dust. In Fig. 1, we see that at high frequencies, N_r tends to N_r^0. In this case, $N_i^0=0$, as expected.

The inclusion of charged dust particles with variable charge in the plasma results in $N_i \neq 0$ and $N_i > 0$, which implies that the wave is spatially absorbed when travelling in the plasma.

We have also estimated the dependence on temperature of quantities that play an important role in the physical description of the process we are studying. The frequencies ν_{ed} and ν_{id}, characterizing the rate of capture of electrons and ions respectively by dust particles in the equilibrium state, and also Z_d, increase with temperature, but n_{e0} and the charging frequency ν_d^0 decrease with temperature. For the parameters used in Figs 1 and 2, the values of ν_{ed}^0/Ω_i and ν_d^0/Ω_i are always localized to the left of the corresponding cutoff frequency. In other words, for $\omega<\omega_c$, we have the possibility that ω can be less than ν_d^0 and $\nu_{\beta d}^0$, which implies that in this range of frequencies, the condition $\omega \gg \max(kv_{Te}, \nu_d^0, \nu_{\beta d}^0)$ is not fulfilled. Then the expansion of denominators that has been made is very bad in this region of the frequency spectrum, and probably leads to the cutoff obtained.

In Figs 3 and 4, we compare numerical results obtained using the expressions for the refractive index of the magnetosonic wave from paper I with those obtained in this paper, in the cold-plasma approximation.

In Fig. 3, the real part of the refractive index in the cold-plasma model is plotted as a function of ω/Ω_i using the two procedures for the calculation. The straight line shows $N_r=N_r^0$ in the cold-plasma model for a plasma without dust. Curve (a) shows N_r calculated using the procedure developed in this paper; curve (b) shows N_r as calculated in paper I. The parameters used are $a=$

https://doi.org/10.1017/S0022377800008448 Published online by Cambridge University Press

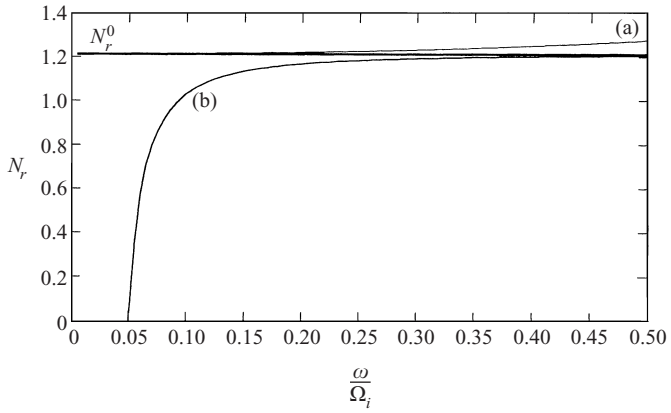


Figure 3. N_r as a function of ω/Ω_i, using the cold-plasma model, the parameters being $a = 10^{-4}$ cm, $n_{i0} = 10^8$ cm^{-3}, $n_{d0} = 10^4$ cm^{-3}, $B_0 = 0.2$ T and $T = 1$ eV. Curve (a) was calculated using the procedure developed in this paper, while curve (b) corresponds to the calculation using the procedure of paper I. The curve N_r^0 corresponds to the refractive index in the absence of dust particles.

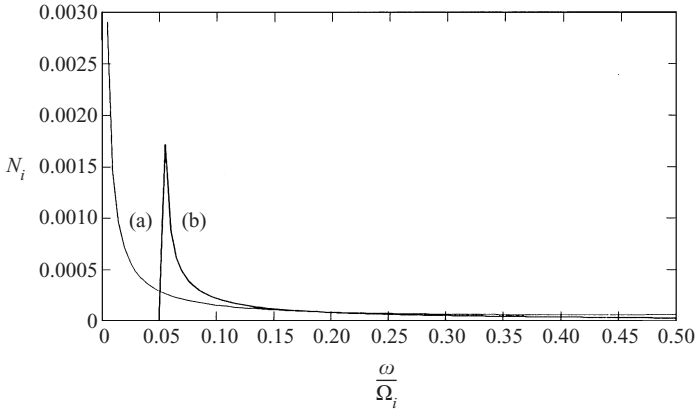


Figure 4. N_i as a function of ω/Ω_i, using the cold-plasma model, for the same parameters and situations presented in Fig. 3.

10^{-4} cm, $n_{i0} = 10^8$ cm^{-3}, $n_{d0} = 10^4$ cm^{-3}, $B_0 = 0.2$ T and $T = 1$ eV. For this set of parameters, we see that the cutoff, which originates from the formulation developed in paper I, does not occur in the region $\Omega_d/\Omega_i \ll \omega/\Omega_i \ll 1$ when we use the procedure developed in this paper. We can say that the approach of paper I is satisfactory for situations where the temperature is not very high, and that the region of agreement between the two methods of calculating N_r increases as the temperature is lowered.

N_r obtained from the calculations of this paper, represented by curve (a), departs from the value of N_r^0 when ω/Ω_i increases. The results from paper I are unable to represent this feature, because we have assumed from the start that $\omega/\Omega_i \ll 1$, in order to make the expansions of the denominators.

In Fig. 4, we present, for the same parameters and situations used in Fig. 3, N_i as a function of ω/Ω_i. The cutoff exhibited by N_r generates a forbidden region of values of N_i in curve (b) obtained from paper I, which does not exist in curve

https://doi.org/10.1017/S0022377800008448 Published online by Cambridge University Press

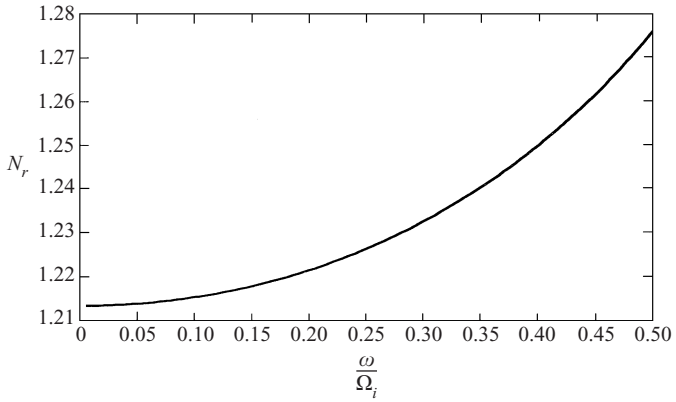


Figure 5. N_r as a function of ω/Ω_i, including Larmor-radius effects. The parameters used are $n_{d0} = 10^4$ cm^{-3}, $n_{i0} = 10^8$ cm^{-3}, $a = 10^{-4}$ cm and $B_0 = 0.2$ T. The same curve is obtained for $T = 0.06$, 0.25 and 1 eV.

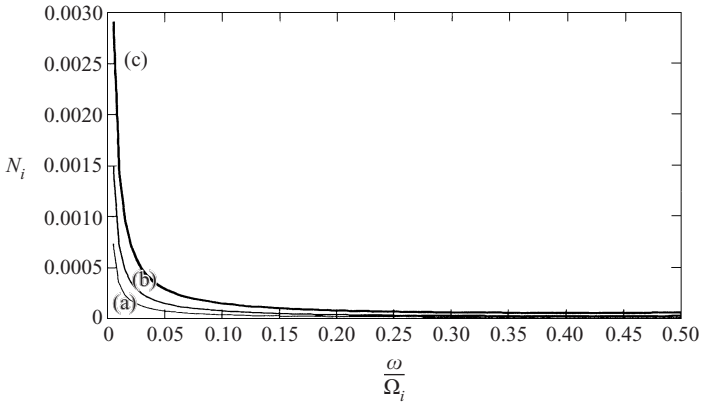


Figure 6. N_i as function of ω/Ω_i, including Larmor-radius effects, using the same parameters as in Fig. 5. The curves labelled by (a), (b) and (c) correspond to $T = 0.06$, 0.25 and 1 eV respectively.

(a). We notice that this result comes from a formulation in which the expansion of the denominators has not been introduced, and in which, therefore, the effects of charge variation are dealt with in a more complete way. Figure 4 shows that the charge variation of the dust particles is more important for lower values of ω/Ω_i.

In Figs 5 and 6, we show N_r and N_i as functions of ω/Ω_i, calculated using the procedure developed in this paper and including Larmor-radius effects of electrons and ions, for $\Omega_d \ll \omega < \Omega_i$. The parameters used are $n_{d0} = 10^4$ cm^{-3}, $n_{i0} = 10^8$ cm^{-3}, $a = 10^{-4}$ cm and $B_0 = 0.2$ T, and the temperatures are (a) $T = 0.06$ eV, (b) $T = 0.25$ eV and (c) $T = 1$ eV.

We see in Fig. 5 that for this set of temperature values, we obtain approximately the same curve for N_r, which departs only slightly, for low values of ω/Ω_i, from the straight line that characterizes the plasma without dust. We can say that N_r is not very sensitive to the charge variation of the dust particles, which is influenced by the temperature, which in turn modifies the frequencies

https://doi.org/10.1017/S0022377800008448 Published online by Cambridge University Press

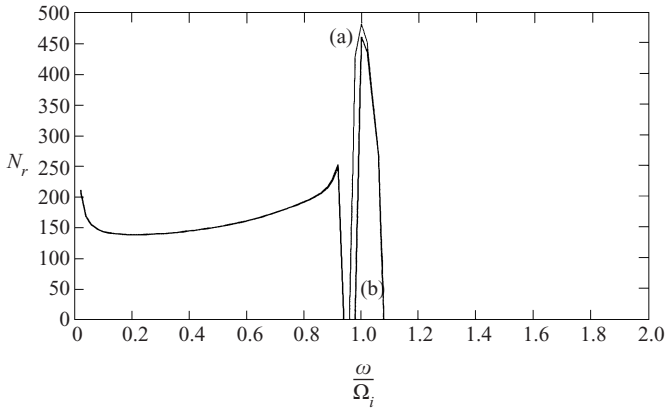


Figure 7. N_r as a function of ω/Ω_i, using the expressions developed in this paper: curve (a) includes Larmor-radius effects; curve (b) is for the cold-plasma model. The parameters used are $n_{i0} = 10^8$ cm^{-3}, $a = 10^{-4}$ cm, $n_{a0} = 10^4$ cm^{-3}, $T = 100$ eV and $B_0 = 10^{-3}$ T.

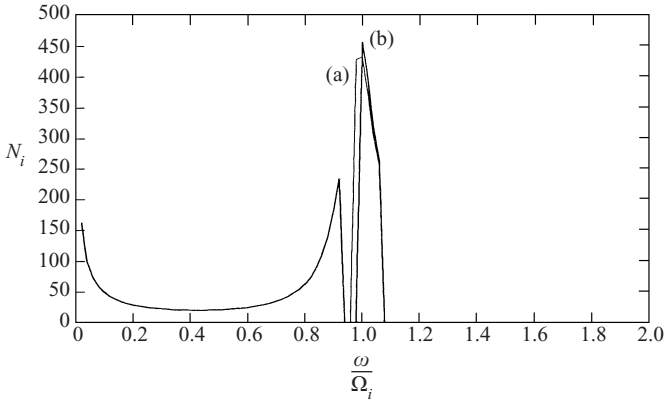


Figure 8. N_i as a function of ω/Ω_i for the same situations and parameters as in Fig. 7.

related to the charging process and also the charging time. We expect that in the frequency region where $\omega \ll \Omega_d$, N_r will be altered more significantly when the temperature is changed, because it is in this region that the characteristic charging frequencies are localized. Also in this frequency region, new wave propagation modes (Rao 1995) will arise owing to the inclusion of the motion of dust particles.

In Fig. 6, we see that for fixed values of ω/Ω_i, N_i increases with increasing temperature. For $\omega/\Omega_i > 0.2$, the values of N_i are approximately equal and very small. Again we observe that the influence of the charge variation of the dust particles is enhanced at low frequencies. We remark that when ω increases relative to the charging frequency ν_d^0, the importance of the charge variation of the dust particles decreases, and accordingly N_i must decrease, because it is directly connected with charge variation.

From the numerical calculation, we observe that the Larmor-radius effects included are negligible in the range of frequencies $\Omega_d \ll \omega < \Omega_i$.

In Figs 7 and 8, we extend the region of variation of the frequency to include frequencies above Ω_i, and compare, using the procedure developed in this paper

https://doi.org/10.1017/S0022377800008448 Published online by Cambridge University Press

to calculate the dielectric tensor, the situation of a cold plasma with a situation where Larmor-radius effects are retained.

In Figs 7 and 8, we show N_r and N_i respectively as functions of ω/Ω_i, with curve (a) corresponding to the situation with Larmor-radius effects included and curve (b) to the cold-plasma limit. The parameters used are $n_{i0} = 10^8$ cm^{-3}, $a = 10^{-4}$ cm, $n_{d0} = 10^4$ cm^{-3}, $T = 100$ eV and $B_0 = 10^{-3}$ T.

We observe that in the range of frequencies $\omega < \Omega_i$, Larmor-radius effects are unimportant, but in the range $\omega \geqslant \Omega_i$, they start to contribute significantly, because for each component of the dielectric tensor, the quantities $\chi_{ij}^{0R}/\chi_{ij}^{1R}$ and $\chi_{ij}^{0I}/\chi_{ij}^{1I}$, which characterize the relative importance of powers of the Larmor radius, are proportional to $Y_\beta \equiv \Omega_\beta/\omega$.

From the numerical calculation, we observe that the dominant contributions of the Larmor radius arise from the 'homogeneous' part of the dielectric tensor (ϵ_{ij}^h). The contributions of order N^2 arising from ϵ_{ij}^N are, for the situations tested, negligible – essentially because the coefficient C, which is a multiplicative factor for all components, is very small.

5. Conclusions

Although in the present paper we have concentrated on the study of a magnetosonic wave, which implies perpendicular propagation, the results of Sect. 2 apply to all directions of propagation. We expect that the contributions due to the charge variation of the dust particles of order N^2, included in ϵ_{ij}^N, can be relevant for parallel propagation of the wave.

Also, if we include the effects of inhomogeneities in the dielectric tensor, we can study the influence of the dust particles with variable charge on Alfvén-wave resonant absorption and in its conversion to a kinetic Alfvén wave. The modification of the Alfvén resonance absorption mechanism due to the presence of charged dust grains was considered by Cramer and Vladimirov (1998). Damping due to the charging of the grains was included in such a way that this corresponds only to the effects included in the part $\tilde{\epsilon}_{ij}^h$ of the dielectric tensor, presented here. For instance, Hasegawa (1976) pointed out that in regions near the resonant point, Larmor-radius effects become important. This suggests that the effects of the charging of the grains included in the part $\tilde{\epsilon}_{ij}^N$ of our tensor would be essential in studying Alfvén resonance absorption. We intend to include the effects of inhomogeneities in our tensor and to apply it to this topic in the future.

Appendix A

In Appendix A of paper I, we presented the quantities $R_{ij}^{n\beta}$ in their general form, as functions of ψ, the angle between the vector $\mathbf{k}_\perp$ and the x axis. For the case of $\psi = 0$, considered in the present paper, the quantities $R_{ij}^{n\beta}$ assume the following forms:

$$R_{xx}^{n\beta} = \frac{n^2}{b_\beta^2} J_n^2(b_\beta), \tag{A 1}$$

$$R_{xy}^{n\beta} = -R_{yx}^{n\beta} = i\frac{n}{b_\beta} J_n(b_\beta) J_n'(b_\beta), \tag{A 2}$$

https://doi.org/10.1017/S0022377800008448 Published online by Cambridge University Press

$$R_{xz}^{n\beta} = R_{zx}^{n\beta} = \frac{n}{b_\beta} J_n^2(b_\beta), \tag{A 3}$$

$$R_{yy}^{n\beta} = J_n'^2(b_\beta), \tag{A 4}$$

$$R_{yz}^{n\beta} = -R_{zy}^{n\beta} = -iJ_n(b_\beta) J_n'(b_\beta), \tag{A 5}$$

$$R_{zz}^{n\beta} = J_n^2(b_\beta), \tag{A 6}$$

where $b_\beta = k_\perp c u_\perp / \Omega_\beta$.

Appendix B

The components of the dielectric tensor $\epsilon_{ij} = \tilde{\epsilon}_{ij}^h + \epsilon_{ij}^N$, in terms of the integrals $\tilde{I}_\beta(n, m, h, s, G)$, are given in the following. The $\tilde{\epsilon}_{ij}^h$ components are written as

$$\tilde{\epsilon}_{xx}^h = 1 + \sum_\beta X_\beta \sum_{n=1}^{\infty} \sum_{m=0}^{\infty} \left(\frac{N_\perp}{Y_\beta}\right)^{2(n+m-1)} n^2 a(n, m)$$

$$\times \sum_{s=\pm 1} \tilde{I}_\beta(n, m, 0, s; \mathscr{L} F_{\beta 0}), \tag{B 1}$$

$$\tilde{\epsilon}_{xy}^h = -i \sum_\beta X_\beta \sum_{n=1}^{\infty} \sum_{m=0}^{\infty} \left(\frac{N_\perp}{Y_\beta}\right)^{2(n+m-1)} n(n+m)\, a(n, m)$$

$$\times \sum_{s=\pm 1} s \tilde{I}_\beta(n, m, 0, s; \mathscr{L} F_{\beta 0}), \tag{B 2}$$

$$\tilde{\epsilon}_{xz}^h = -\sum_\beta X_\beta \frac{N_\perp}{Y_\beta} \sum_{n=1}^{\infty} \sum_{m=0}^{\infty} \left(\frac{N_\perp}{Y_\beta}\right)^{2(n+m-1)} n a(n, m)$$

$$\times \sum_{s=\pm 1} s \left[\tilde{I}_\beta(n, m, 1, s; \mathscr{L} F_{\beta 0}) + \tilde{I}_\beta\left(n, m, 0, s; \frac{i\nu_{\beta d}^0}{\omega} L F_{\beta 0}\right)\right], \tag{B 3}$$

$$\tilde{\epsilon}_{yy}^h = 1 + \sum_\beta X_\beta \sum_{m=2}^{\infty} \left(\frac{N_\perp}{Y_\beta}\right)^{2(m-1)} d(0, m)\, \tilde{I}_\beta(0, m, 0, 0; \mathscr{L} F_{\beta 0})$$

$$+ \sum_\beta X_\beta \sum_{n=1}^{\infty} \sum_{m=0}^{\infty} \left(\frac{N_\perp}{Y_\beta}\right)^{2(n+m-1)} d(n, m) \sum_{s=\pm 1} \tilde{I}_\beta(n, m, 0, s; \mathscr{L} F_{\beta 0}), \tag{B 4}$$

$$\tilde{\epsilon}_{yz}^h = -i \sum_\beta X_\beta \frac{N_\perp}{Y_\beta} \sum_{m=1}^{\infty} \left(\frac{N_\perp}{Y_\beta}\right)^{2(m-1)} m a(0, m)$$

$$\times \left[\tilde{I}_\beta(0, m, 1, 0; \mathscr{L} F_{\beta 0}) + \tilde{I}_\beta\left(0, m, 0, s; \frac{i\nu_{\beta d}^0}{\omega} L F_{\beta 0}\right)\right]$$

$$-i \sum_\beta X_\beta \frac{N_\perp}{Y_\beta} \sum_{n=1}^{\infty} \sum_{m=0}^{\infty} \left(\frac{N_\perp}{Y_\beta}\right)^{2(n+m-1)} (n+m)\, a(n, m)$$

$$\times \sum_{s=\pm 1} \left[\tilde{I}_\beta(n, m, 1, s; \mathscr{L} F_{\beta 0}) + \tilde{I}_\beta\left(n, m, 0, s; \frac{i\nu_{\beta d}^0}{\omega} L F_{\beta 0}\right)\right], \tag{B 5}$$

https://doi.org/10.1017/S0022377800008448 Published online by Cambridge University Press

$$\tilde{\epsilon}^h_{zz} = 1 + \sum_\beta X_\beta \tilde{I}_\beta\left(0,0,1,0; u_\perp \frac{\partial F_{\beta 0}}{\partial u_\parallel}\right)$$

$$+ \sum_\beta X_\beta \sum_{m=1}^{\infty} \left(\frac{N_\perp}{Y_\beta}\right)^{2m} a(0,m)$$

$$\times \left[\tilde{I}_\beta(0,m,2,0; \mathscr{L} F_{\beta 0}) + \tilde{I}_\beta\left(0,m,1,0; \frac{i\nu^0_{\beta d}}{\omega} L F_{\beta 0}\right)\right]$$

$$+ \sum_\beta X_\beta \sum_{n=1}^{\infty} \sum_{m=0}^{\infty} \left(\frac{N_\perp}{Y_\beta}\right)^{2(n+m)} a(n,m)$$

$$\times \sum_{s=\pm 1} \left[\tilde{I}_\beta(n,m,2,s; \mathscr{L} F_{\beta 0}) + \tilde{I}_\beta\left(n,m,1,s; \frac{i\nu^0_{\beta d}}{\omega} L F_{\beta 0}\right)\right], \tag{B 6}$$

and $\tilde{\epsilon}^h_{ji} = (\tilde{\epsilon}^h_{ij})^*$.

Similarly, the ϵ^N_{ij} components are written as

$$\epsilon^N_{ij} = -\frac{i}{\omega}\frac{c^2}{\omega^2} \frac{1}{1 + i\left(\frac{\nu^0_d}{\omega} + \frac{\nu_1}{\omega}\right)} U_i S_j, \tag{B 7}$$

where

$$U_x = -\sum_\beta q_\beta n_{\beta 0} \sum_{n=1}^{\infty} \sum_{m=0}^{\infty} n a(n,m) \left(\frac{N_\perp}{Y_\beta}\right)^{2(n+m)-1}$$

$$\times \sum_{s=\pm 1} s \tilde{I}_\beta(n,m,0,s; u\sigma'_\beta u_\perp F_{\beta 0}), \tag{B 8}$$

$$U_y = -i \sum_\beta q_\beta n_{\beta 0} \left[\sum_{m=1}^{\infty} m a(0,m) \left(\frac{N_\perp}{Y_\beta}\right)^{2m-1} \tilde{I}_\beta(0,m,0,0; u\sigma'_\beta u_\perp F_{\beta 0})\right.$$

$$\left. + \sum_{n=1}^{\infty} \sum_{m=0}^{\infty} (n+m)\, a(n,m) \left(\frac{N_\perp}{Y_\beta}\right)^{2(n+m)-1} \sum_{s=\pm 1} \tilde{I}_\beta(n,m,0,s; u\sigma'_\beta u_\perp F_{\beta 0})\right], \tag{B 9}$$

$$U_z = \sum_\beta q_\beta n_{\beta 0} \left[\sum_{m=0}^{\infty} a(0,m) \left(\frac{N_\perp}{Y_\beta}\right)^{2m} \tilde{I}_\beta(0,m,1,0; u\sigma'_\beta u_\perp F_{\beta 0})\right.$$

$$\left. + \sum_{n=1}^{\infty} \sum_{m=0}^{\infty} a(n,m) \left(\frac{N_\perp}{Y_\beta}\right)^{2(n+m)} \sum_{s=\pm 1} \tilde{I}_\beta(n,m,1,s; u\sigma'_\beta u_\perp F_{\beta 0})\right], \tag{B 10}$$

$$S_x = -\sum_\beta \frac{\omega^2_{p\beta}}{c} \sum_{n=1}^{\infty} \sum_{m=0}^{\infty} n a(n,m) \left(\frac{N_\perp}{Y_\beta}\right)^{2(n+m)-1}$$

$$\times \sum_{s=\pm 1} s \tilde{I}_\beta\left(n,m,0,s; i\frac{\nu^0_{\beta d}}{\omega} \gamma_\beta \mathscr{L} F_{\beta 0}\right), \tag{B 11}$$

https://doi.org/10.1017/S0022377800008448 Published online by Cambridge University Press

$$S_y = i\sum_\beta \frac{\omega_{p\beta}^2}{c}\Bigg[\sum_{m=1}^{\infty} ma(0,m)\left(\frac{N_\perp}{Y_\beta}\right)^{2m-1}\tilde{I}_\beta\left(0,m,0,0;i\frac{\nu_{\beta d}^0}{\omega}\gamma_\beta \mathscr{L}F_{\beta 0}\right)$$
$$+\sum_{n=1}^{\infty}\sum_{m=0}^{\infty}(n+m)\,a(n,m)\left(\frac{N_\perp}{Y_\beta}\right)^{2(n+m)-1}$$
$$\times\sum_{s=\pm 1}\tilde{I}_\beta\left(n,m,0,s;i\frac{\nu_{\beta d}^0}{\omega}\gamma_\beta \mathscr{L}F_{\beta 0}\right)\Bigg], \tag{B 12}$$

$$S_z = \sum_\beta \frac{\omega_{p\beta}^2}{c}\left[\tilde{I}_\beta\left(0,0,0,0;i\frac{\nu_{\beta d}^0}{\omega}u_\perp\frac{\partial F_{\beta 0}}{\partial u_\parallel}\right)-2\tilde{I}_\beta\left(0,0,0,0;\left(i\frac{\nu_{\beta d}^0}{\omega}\right)^2 LF_{\beta 0}\right)\right]$$
$$+\sum_\beta \frac{\omega_{p\beta}^2}{c}\sum_{m=1}^{\infty}\left(\frac{N_\perp}{Y_\beta}\right)^{2m}a(0,m)$$
$$\times\left[\tilde{I}_\beta\left(0,m,1,0;i\frac{\nu_{\beta d}^0}{\omega}\mathscr{L}F_{\beta 0}\right)-\tilde{I}_\beta\left(0,m,0,0;\left(i\frac{\nu_{\beta d}^0}{\omega}\right)^2 LF_{\beta 0}\right)\right]$$
$$+\sum_\beta \frac{\omega_{p\beta}^2}{c}\sum_{n=1}^{\infty}\sum_{m=0}^{\infty}\left(\frac{N_\perp}{Y_\beta}\right)^{2(n+m)}a(n,m)$$
$$\times\sum_{s=\pm 1}\left[\tilde{I}_\beta\left(n,m,1,s;i\frac{\nu_{\beta d}^0}{\omega}\mathscr{L}F_{\beta 0}\right)-\tilde{I}_\beta\left(n,m,0,s;\left(i\frac{\nu_{\beta d}^0}{\omega}\right)^2 LF_{\beta 0}\right)\right]. \tag{B 13}$$

The parameter ν_1 is given by

$$\nu_1 = c\sum_\beta q_\beta n_{\beta 0}\Bigg[\sum_{m=0}^{\infty}a(0,m)\left(\frac{N_\perp}{Y_\beta}\right)^{2m}\tilde{I}_\beta\left(0,m,0,0;i\frac{\nu_{\beta d}^0}{\omega}\gamma_\beta u_\perp u\sigma'_\beta F_{\beta 0}\right)$$
$$+\sum_{n=1}^{\infty}\sum_{m=0}^{\infty}a(n,m)\left(\frac{N_\perp}{Y_\beta}\right)^{2(n+m)}\sum_{s=\pm 1}\tilde{I}_\beta\left(n,m,0,s;i\frac{\nu_{\beta d}^0}{\omega}\gamma_\beta u_\perp u\sigma'_\beta F_{\beta 0}\right)\Bigg], \tag{B 14}$$

and ν_d^0 is given by (2.9).

Appendix C

The expressions for χ_{ij}^{0R}, χ_{ij}^{0I}, χ_{ij}^{1R} and χ_{ij}^{1I} are as follows:

$$\chi_{xx}^{0R} = -\frac{1}{3(2\pi)^{1/2}}\Bigg\{X_i\mu_i^{5/2}[(1+Y_i)I(1,6)+(1-Y_i)I(-1,6)]$$
$$+X_e\mu_e^{5/2}\left[(1+Y_e)E(1,6)+(1-Y_e)E(-1,6)+\frac{2}{1-Y_e^2}i_4\right]\Bigg\}, \tag{C 1}$$

$$\chi_{xx}^{1R} = -\frac{1}{15(2\pi)^{1/2}}\Bigg\{\frac{X_i\mu_i^{5/2}}{Y_i^2}[(1+2Y_i)I(2,8)+(1-2Y_i)I(-2,8)$$
$$-(1+Y_i)I(1,8)-(1-Y_i)I(-1,8)]$$
$$+\frac{X_e\mu_e^{5/2}}{Y_e^2}\left[(1+2Y_e)E(2,8)+(1-2Y_e)E(-2,8)+\frac{2}{1-4Y_e^2}i_6-\frac{2}{1-Y_e^2}i_6\right.$$
$$\left.-(1+Y_e)E(1,8)-(1-Y_e)E(-1,8)\right]\Bigg\}, \tag{C 2}$$

https://doi.org/10.1017/S0022377800008448 Published online by Cambridge University Press

$$\chi_{xx}^{0I} = \frac{A}{3(2\pi)^{1/2}}\{X_i\mu_i^{5/2}[I(1,7)+\tilde{C}_i I(1,5)+I(-1,7)+\tilde{C}_i I(-1,5)]$$
$$+X_e\mu_e^{5/2}[E(1,7)+\tilde{C}_e E(1,5)+E(-1,7)+\tilde{C}_e E(-1,5)]\}, \tag{C 3}$$

$$\chi_{xx}^{1I} = \frac{A}{15(2\pi)^{1/2}}\left\{\frac{X_i\mu_i^{5/2}}{Y_i^2}[I(2,9)+\tilde{C}_i I(2,7)+I(-2,9)+\tilde{C}_i I(-2,7)\right.$$
$$-I(1,9)-\tilde{C}_i I(1,7)-I(-1,9)-\tilde{C}_i I(-1,7)]$$
$$+\frac{X_e\mu_e^{5/2}}{Y_e^2}[E(2,9)+\tilde{C}_e E(2,7)+E(-2,9)+\tilde{C}_e E(-2,7)$$
$$\left.-E(1,9)-\tilde{C}_e E(1,7)-E(-1,9)-\tilde{C}_e E(-1,7)]\right\}, \tag{C 4}$$

$$\chi_{yy}^{1R} = -\frac{2}{15(2\pi)^{1/2}}\left\{\frac{X_i\mu_i^{5/2}}{Y_i^2}[2I(0,8)-(1+Y_i)I(1,8)-(1-Y_i)I(-1,8)]\right.$$
$$+\frac{X_e\mu_e^{5/2}}{Y_e^2}\left[2E(0,8)-(1+Y_e)E(1,8)-(1-Y_e)E(-1,8)\right.$$
$$\left.\left.+2i_6-\frac{2}{1-Y_e^2}i_6\right]\right\}, \tag{C 5}$$

$$\chi_{yy}^{1I} = \frac{2A}{15(2\pi)^{1/2}}\left\{\frac{X_i\mu_i^{5/2}}{Y_i^2}[2(I(0,9)+\tilde{C}_i I(0,7))-I(1,9)-\tilde{C}_i I(1,7)\right.$$
$$-I(-1,9)-\tilde{C}_i I(-1,7)]$$
$$+\frac{X_e\mu_e^{5/2}}{Y_e^2}[2(E(0,9)+\tilde{C}_e E(0,7))-E(1,9)-\tilde{C}_e E(1,7)$$
$$\left.-E(-1,9)-\tilde{C}_e E(-1,7)]\right\}, \tag{C 6}$$

$$\chi_{xy}^{0R} = \frac{A}{3(2\pi)^{1/2}}\{X_i\mu_i^{5/2}[I(1,7)+\tilde{C}_i I(1,5)-I(-1,7)-\tilde{C}_i I(-1,5)]$$
$$+X_e\mu_e^{5/2}[E(1,7)+\tilde{C}_e E(1,5)-E(-1,7)-\tilde{C}_e E(-1,5)]\}, \tag{C 7}$$

$$\chi_{xy}^{1R} = \frac{A}{15(2\pi)^{1/2}}\left\{\frac{X_i\mu_i^{5/2}}{Y_i^2}\{I(2,9)+\tilde{C}_i I(2,7)-I(-2,9)-\tilde{C}_i I(-2,7)\right.$$
$$-2[I(1,9)+\tilde{C}_i I(1,7)+2I(-1,9)+\tilde{C}_i I(-1,7)]\}$$
$$+\frac{X_e\mu_e^{5/2}}{Y_e^2}\{E(2,9)+\tilde{C}_e E(2,7)-E(-2,9)-\tilde{C}_e E(-2,7)$$
$$\left.-2[E(1,9)+\tilde{C}_e E(1,7)+2E(-1,9)+\tilde{C}_e E(-1,7)]\}\right\}, \tag{C 8}$$

$$\chi_{xy}^{0I} = \frac{1}{3(2\pi)^{1/2}}\left\{X_i\mu_i^{5/2}[(1+Y_i)I(1,6)-(1-Y_i)I(-1,6)]\right.$$
$$\left.+X_e\mu_e^{5/2}\left[(1+Y_e)E(1,6)-(1-Y_e)E(-1,6)-\frac{2Y_e}{1-Y_e^2}i_4\right]\right\}, \tag{C 9}$$

https://doi.org/10.1017/S0022377800008448 Published online by Cambridge University Press

$$\chi_{xy}^{1I} = \frac{1}{15(2\pi)^{1/2}}\left\{\frac{X_i\mu_i^{5/2}}{Y_i^2}[(1+2Y_i)I(2,8)-(1-2Y_i)I(-2,8)\right.$$
$$-2(1+Y_i)I(1,8)+2(1-Y_i)I(-1,8)]$$
$$+\frac{X_e\mu_e^{5/2}}{Y_e^2}\left[(1+2Y_e)E(2,8)-(1-2Y_e)E(-2,8)\right.$$
$$-2(1+Y_e)E(1,8)+2(1-Y_e)E(-1,8)$$
$$\left.\left.-\frac{4Y_e}{1-4Y_e^2}i_6+\frac{4Y_e}{1-Y_e^2}i_6\right]\right\}. \tag{C 10}$$

Appendix D

The full expressions for the F_{ij}^R and F_{ij}^I are as follows:

$$F_{ij}^R = u_i^R s_j^R - u_i^I s_j^I, \tag{D 1}$$
$$F_{ij}^I = u_i^R s_j^I + u_i^I s_j^R, \tag{D 2}$$

with

$$u_x^R = \frac{\omega_{pi}^2\mu_i^{3/2}}{Y_i}[(1+Y_i)I(1,5)-(1-Y_i)I(-1,5)]$$
$$+\frac{\omega_{pe}^2\mu_e^{3/2}}{Y_e}[(1+Y_e)E(1,5)-(1-Y_e)E(-1,5)], \tag{D 3}$$

$$u_x^I = -A\left\{\frac{\omega_{pi}^2\mu_i^{3/2}}{Y_i}[I(1,6)+\tilde{C}_iI(1,4)-I(-1,6)-\tilde{C}_iI(-1,4)]\right.$$
$$\left.+\frac{\omega_{pe}^2\mu_e^{3/2}}{Y_e}[E(1,6)+\tilde{C}_eE(1,4)-E(-1,6)-\tilde{C}_eE(-1,4)]\right\}, \tag{D 4}$$

$$s_x^R = \frac{\omega_{pi}^2\mu_i^{5/2}}{Y_i}\{(1+Y_i)[I(1,7)+\tilde{C}_iI(1,5)]$$
$$-(1-Y_i)[I(-1,7)+\tilde{C}_iI(-1,5)]\}$$
$$+\frac{\omega_{pe}^2\mu_e^{5/2}}{Y_e}\{(1+Y_e)[E(1,7)+\tilde{C}_eE(1,5)]$$
$$-(1-Y_e)[E(-1,7)+\tilde{C}_eE(-1,5)]\}, \tag{D 5}$$

$$s_x^I = -A\left\{\frac{\omega_{pi}^2\mu_i^{5/2}}{Y_i}[I(1,8)+2\tilde{C}_iI(1,6)+\tilde{C}_i^2I(1,4)\right.$$
$$-I(-1,8)-2\tilde{C}_iI(-1,6)-\tilde{C}_i^2I(-1,4)]$$
$$+\frac{\omega_{pe}^2\mu_e^{5/2}}{Y_e}[E(1,8)+2\tilde{C}_eE(1,6)+\tilde{C}_e^2E(1,4)$$
$$\left.-E(-1,8)-2\tilde{C}_eE(-1,6)-\tilde{C}_e^2E(-1,4)]\right\}, \tag{D 6}$$

$$u_y^R = \frac{\omega_{pi}^2\mu_i^{3/2}}{Y_i}[2I(0,5)-(1+Y_i)I(1,5)-(1-Y_i)I(-1,5)]$$
$$+\frac{\omega_{pe}^2\mu_e^{3/2}}{Y_e}[2E(0,5)-(1+Y_e)E(1,5)-(1-Y_e)E(-1,5)], \tag{D 7}$$

https://doi.org/10.1017/S0022377800008448 Published online by Cambridge University Press

$$u_y^I = -A\Bigg\{\frac{\omega_{pi}^2\mu_i^{3/2}}{Y_i}\{2[I(0,6)+\tilde{C}_i I(0,4)]-I(1,6)-\tilde{C}_i I(1,4) -I(-1,6)-\tilde{C}_i I(-1,4)\} +\frac{\omega_{pe}^2\mu_e^{3/2}}{Y_e}\{2[E(0,6)+\tilde{C}_e E(0,4)]-E(1,6)-\tilde{C}_e E(1,4) -E(-1,6)-\tilde{C}_e E(-1,4)\}\Bigg\}, \tag{D 8}$$

$$s_y^R = \frac{\omega_{pi}^2\mu_i^{5/2}}{Y_i}\{-2[I(0,7)+\tilde{C}_i I(0,5)] +(1+Y_i)\,[I(1,7)+\tilde{C}_i I(1,5)]+(1-Y_i)\,[I(-1,7)+\tilde{C}_i I(-1,5)]\} +\frac{\omega_{pe}^2\mu_e^{5/2}}{Y_e}\{-2[E(0,7)+\tilde{C}_e E(0,5)] +(1+Y_e)\,[E(1,7)+\tilde{C}_e E(1,5)]+(1-Y_e)\,[E(-1,7)+\tilde{C}_e E(-1,5)]\}, \tag{D 9}$$

$$s_y^I = -A\Bigg\{\frac{\omega_{pi}^2\mu_i^{5/2}}{Y_i}\{-2[I(0,8)+2\tilde{C}_i I(0,6)+\tilde{C}_i^2 I(0,4)] +I(1,8)+2\tilde{C}_i I(1,6)+\tilde{C}_i^2 I(1,4) +I(-1,8)+2\tilde{C}_i I(-1,6)+\tilde{C}_i^2 I(-1,4)\} +\frac{\omega_{pe}^2\mu_e^{5/2}}{Y_e}\{-2[E(0,8)+2\tilde{C}_e E(0,6)+\tilde{C}_e^2 E(0,4)] +E(1,8)+2\tilde{C}_e E(1,6)+\tilde{C}_e^2 E(1,4) +E(-1,8)+2\tilde{C}_e E(-1,6)+\tilde{C}_e^2 E(-1,4)\}\Bigg\}. \tag{D 10}$$

References

Abramowitz, M. and Stegun, I. A. 1970 *Handbook of Mathematical Functions*. Dover, New York.

Chang, J. S. and Spariosu, K. 1993 Dust particle charging characteristics under a collisionless magneto-plasma. *J. Phys. Soc. Japan* **62**, 97.

Cramer, N. F. and Vladimirov, S. V. 1998 The resonance absorption of wave energy in a dusty plasma. *Physica Scripta* **T45**, 213.

de Juli, M. C. and Schneider, R. S. 1998 The dielectric tensor for dusty magnetized plasmas with variable charge on dust particles. *J. Plasma Phys.* **60**, 243.

Hasegawa, A. 1976 Kinetic processes in plasma heating by resonant mode conversion of Alfvén wave. *Phys. Fluids* **19**, 1924.

Prasad, P. V. S. R. 1998 Acoustic modes in a dusty plasma. *Phys. Lett.* **239A**, 378.

Rao, N. N. 1995 Magnetoacoustic modes in a magnetized dusty plasma. *J. Plasma Phys.* **53**, 317.

Spitzer, L. J. 1978 *Physical Processes in the Interstellar Medium*. Wiley, New York.

Tsytovich, V. N. 1997 Dust plasma crystals, drops and clouds. *Soviet Phys. Usp.* **40**, 53.

Vladimirov, S. V. 1994 Propagation of waves in dusty plasmas with variable charges on dust particles. *Phys. Plasmas* **1**, 2762.

https://doi.org/10.1017/S0022377800008448 Published online by Cambridge University Press